# Scattered-wave integral-transform method of holographic-image reconstruction from forward-scattering diffraction patterns

B. P. Tonner, Zhi-Lan Han, G. R. Harp, and D. K. Saldin
*Department of Physics, University of Wisconsin-Milwaukee, 1900 East Kenwood Blvd., Milwaukee, Wisconsin 53211*
(Received 11 February 1991)

Forward-scattering holography has advantages for the study of the structure of subsurface atoms, but early results reveal the need for image-correction techniques to compensate for the angular dependence of the scattered waves which are the object waves of the photoelectron hologram. We have developed a generalized integral transform for image reconstruction, with a kernel derived from the single-scattering wave functions, that includes the effects of the angular variation of the atomic-scattering-factor amplitude and phase, as well as matrix-element effects that appear in the scattered object waves. This method for scattering-factor corrections preserves the direct-inversion principle of holographic transforms and does not require *a priori* knowledge of atomic positions. In the limit of pure *s*-wave scattering, the scattered-wave-included Fourier transform reduces to a simple phased Fourier transform. It can also be approximately described as a generalized deconvolution which uses a function with six degrees of freedom (momentum and position) derived from the scattered wave functions.

## I. IMAGE ABERRATIONS IN FORWARD-SCATTERING HOLOGRAPHY

The diffraction limit of spatial resolution in a holographic reconstruction, $\delta r \sim \pi/|\mathbf{k}|$, suggests that a way to improve the accuracy of the image is to use electrons with high kinetic energies. An additional benefit of increased kinetic energy is a longer electron mean free path, which makes it possible to get images of atoms lying below the surface. As the kinetic energy of a diffracting electron is raised above a few hundred electron volts, the atomic scattering factor becomes increasingly anisotropic, showing both a strongly peaked amplitude in the forward-scattering direction, and a large variation of the phase with scattering angle. The angular dependence of the scattering factor affects the form of the scattered waves that are the object waves of the photoemission hologram. This leads to additional subtleties in the interpretation of forward-scattering photoemission holograms.[1-7]

Experimental studies of single-crystal[1,2,7] and ultrathin film[3] forward-scattering geometry holograms have demonstrated that atomic-resolution real-space images can be produced from diffraction patterns collected over a substantial portion of $2\pi$ steradian solid angle, at near-kilovolt kinetic energy. Single-crystal holograms give images with high intensity near the correct locations of atoms in the sample in planar reconstructions parallel to the surface, and in radial image plots along near-neighbor bond axes.[2,4] The radial image function (see below, and Ref. 2) has peaks at the correct location for atoms, with no "false atoms" at large radii. Large peaks in the radial image function near the origin have been found to be due in part to an artifact of the zeroth-order diffraction peaks in the forward-scattering diffraction pattern.[4,8]

In planar sections perpendicular to the sample surface, forward-scattering holographic reconstructions show elongated ellipsoidal tubes of intensity near the correct atom positions, with the tubes aligned along the internuclear axis connecting the emitter and scattering atoms. This effect is the result of having the holographic fringes localized in a small angular region of the diffraction pattern, surrounding the forward-scattering direction.[1,2] In the absence of strong forward-scattering peaks, the atom image is elongated parallel to the sample normal, since the range of momentum in the $\hat{\mathbf{z}}$ direction is half that parallel to the surface.[1,7,9]

Perhaps unexpectedly, the high quality of single-crystal images is a direct result of the large amount of multiple forward-scattering paths that contribute to the diffraction pattern and reduce the overall impact of the forward-scattering zero-order diffraction peaks, as noted by Fadley.[10] In Fig. 1 we show a multiple-scattering calculation for a chain of Cu atoms, embedded in an isotropic absorber.[11] The diffraction from an atom near the surface (shown as the two-atom chain result) has a very strong forward-scattering feature. As more emitter atoms are added to the diffraction pattern (simulating a film of increasing thickness), the relative contribution of the forward-scattering peak is reduced in comparison to the oscillating fringes at larger scattering angles, due to the effects of multiple forward scattering along the chain axis. These fringes are the important component of the hologram for Fourier-transform image reconstruction, and it is seen that these fringes are reinforced as multiple emitter atoms in equivalent positions are added to the chain.

Real-space images have been obtained from the oscilla-

 

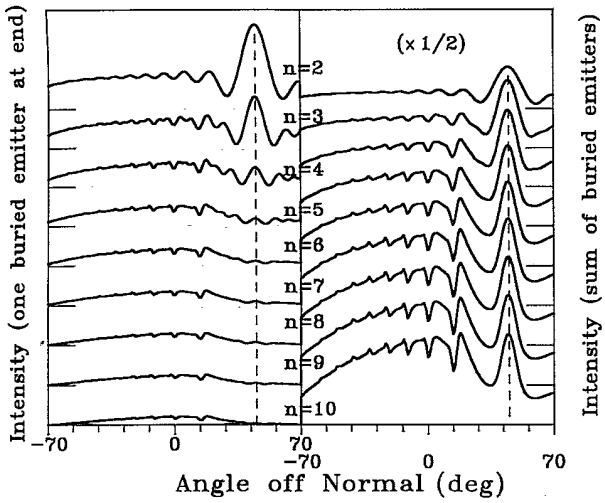


FIG. 1. Multiple-scattering calculation of the Auger electron angular distribution for emitter atoms at different depths in a solid. The model consists of a linear chain of Cu atoms embedded in an isotropic absorber with a surface. The kinetic energy of Cu *LVV* Auger electrons was assumed.

tory part of the forward-scattering diffraction patterns, $\chi(\mathbf{k})$, called the anisotropy,[12–15] which is viewed as resulting from the interference between the direct wave from the emitted atom (the reference wave) and the waves scattered from near-neighbor atoms (the object waves). We have used a slightly modified form of the phased Fourier-integral introduced by Barton:[9]

$$\Phi(\mathbf{r})=\int a(\hat{\mathbf{k}})\chi(\hat{\mathbf{k}})e^{i\mathbf{k}\cdot\mathbf{r}}d\Omega_{\hat{\mathbf{k}}} . \tag{1}$$

The factor $a(\hat{\mathbf{k}})$ is an apodizing function that is introduced to reduce the influence of the Gibbs effect on the final image, $|\Phi(\mathbf{r})|^2$, which arises from the finite range of integration in momentum space.

The physical meaning of the "image function" $\Phi(\mathbf{r})$ can be understood from some simple arguments.[16] If we neglect effects such as refraction or reflection at the surface, the diffraction pattern can be considered to be a map of the final state wave function, $\psi_f(\mathbf{r})$ in momentum space. Let the momentum space wave function be normalized so that its angular average is $\int|\langle\mathbf{k}|\psi_f\rangle|^2d\Omega=4\pi$. Then the anisotropy of the diffraction pattern has the form

$$\chi(\hat{\mathbf{k}})=|\langle\mathbf{k}|\psi_f(\mathbf{r})\rangle|^2-1 . \tag{2}$$

The *three-dimensional* Fourier transform of $|\langle\mathbf{k}|\psi_f(\mathbf{r})\rangle|^2$ is just the autocorrelation of the original final-state wave function. With this as a guide, we can look for a similar interpretation of the high-energy limit of the phase Fourier transform [Eq. (1)] of the final-state wave function. Given certain simplifications[17] that allow the range of integration to extend over $4\pi$ solid angle, it is easy to see that the image function is closely related to the final-state autocorrelation:

$$\Phi(\mathbf{r})=4\pi\left[\int\int\psi_f^*(\mathbf{r}'')\psi_f(\mathbf{r}')\frac{\sin(|\mathbf{k}|\,|\mathbf{r}'-\mathbf{r}''-\mathbf{r}|)}{|\mathbf{k}|\,|\mathbf{r}'-\mathbf{r}''-\mathbf{r}|}d^3\mathbf{r}''d^3\mathbf{r}'-\frac{\sin(|\mathbf{k}|\,|\mathbf{r}|)}{|\mathbf{k}|\,|\mathbf{r}|}\right]$$
$$\sim 4\pi\left[\int\psi_f^*(\mathbf{r}'')\psi_f(\mathbf{r}''+\mathbf{r})d^3\mathbf{r}''-\delta_{\mathbf{r},0}\right] , \quad \text{as } k\to\infty . \tag{3}$$

If the *scattered* waves that make up the final-state wave function are also *s*-like, then from symmetry considerations the autocorrelation of the wave function [Eq. (3)] will have intensity maxima for offset vectors r corresponding to atomic nuclei. For more complex scattered waves, the identification of maxima in $|\Phi(\mathbf{r})|^2$ with the geometric *structure* is not immediately obvious. Nevertheless, we point out that the autocorrelation function contains important structural information that is different from that available by other techniques. In particular, the holographic image function $\Phi^2$ is quite different from the Patterson function of x-ray scattering, a difference that is ultimately a result of the difference between the diffraction patterns formed by a localized "reference" wave and an external plane wave.[18]

Both the forward-scattering holography experiments[1–3] and numerical simulations[3,7] have shown that there are considerable differences in the results of holograpic imaging from single crystals and very thin films. In thin films (or small clusters), single-scattering paths are the major contributions to the diffraction pattern, so that at high kinetic energy the forward-scattering peaks are very large. The angular variation of the atomic scattering factor is responsible for the scattered waves having large peaks in the forward-scattering direction.[19] This angular anisotropy of the scattered waves in turn leads to aberrations in the thin-film images. The two primary aberrations are an atom shift and image asymmetry or broadening. These two effects are illustrated by multiple-scattering calculations[3,7,20,21] for a single emitter atom at the end of a linear chain of copper atoms, shown in Fig. 2. The atom shift can be traced to the angular variation of the phase shift, and the asymmetry arises from the scattering-factor amplitude envelope.[3] The zeroth-order forward-scattering peak itself introduces artifacts in the holographic image that appear *near the origin* of the reconstruction.[4]

These have led us to introduce an improved Fourier-

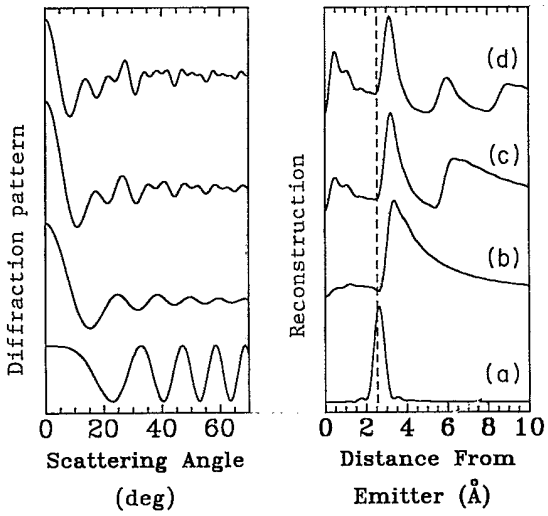


FIG. 2. Angular diffraction patterns (left) and holographic reconstructions (right) for atom chains, simulating Auger emission from Cu at 914 eV. The pattern at the bottom is the "ideal" angular profile for pure $s$-wave scattering; the reconstruction at the right shows the $|\sin[k(r-r_j)]/(r-r_j)|^2$ behavior of an $s$-wave hologram, which has a symmetric shape and maximum at the correct location. The multiple-scattering calculation for two-, three-, and four-atom-long chains is shown in sequence above the ideal model. As more atoms are added to the chain, the forward-scattering feature becomes less prominant, and the image maximum moves towards the correct location.

transform algorithm, which preserves the basic goal of a direct transform method that produces a three-dimensional image from the two-dimensional diffraction pattern. For images reconstructed from diffraction patterns at a single kinetic energy, one form of the generalized holographic integral[22] can be written.[3,7]

$$\Phi(\mathbf{r})=\int \frac{1}{\mathcal{F}(\mathbf{k},\mathbf{r})} a(\hat{\mathbf{k}})\chi(\hat{\mathbf{k}})e^{i\mathbf{k}\cdot\mathbf{r}}d\Omega_{\hat{\mathbf{k}}} . \quad (4)$$

The factor $\mathcal{F}(\mathbf{k},\mathbf{r})$ contains the angular dependence of the scattered waves arising from the atomic scattering factor, as well as angular factors from the emitted wave and scattered waves due to the dipole matrix element. This form of the scattered-wave integral transform is valid in the plane-wave and point-scattering approximations of electron scattering, for which the general integral transform [Eq. (11) below] reduces to a generalized Fourier integral.

The effect of the scattered-wave included Fourier-transform [Eq. (4)] algorithm is to remove the atom shift and anisotropy which is due to the angular dependence of the direct reference wave and the scattered object waves. Application of this transform produces a three-dimensional image with peaks at the correct atom locations and atom sizes near the diffraction limit. The transform does not require prior knowledge of the atom positions. Since the transform corrects the image line shape and position, and does not require initial assumptions about atom positions, we have previously described this algorithm as the "scattered-wave deconvolution method" of holographic imaging.[3,7]

The need for such corrections can be seen in Fig. 3(a). We show the holographic images reconstructed from a model of a two-layer thick Cu(111) film, calculated with a full multiple-scattering cluster theory.[7,20,21] The images are in a plane containing the atoms above the emitter atom, parallel to the surface. The top image was created using the simple phased Fourier integral transform of Eq. (1), with $a(\hat{\mathbf{k}})=\hat{\mathbf{k}}\cdot\hat{\mathbf{n}}$, where $\hat{\mathbf{n}}$ is the normal to the crystal surface. The image contains large areas of high intensity surrounding the correct atom locations, which are marked by white crosses. It is certainly true that such an image can be useful in determining the structure of a thin film. In particular, it immediately determines the local symmetry and approximate location of atoms surrounding the emitter, without the necessity of comparing the actual diffraction pattern to a calculation. However, the spatial resolution is very poor in the (simulated) thin-film image, and the maximum intensity is displaced radially outwards from the origin (see also the experimental images in Ref. 3).

Both the atom shift and the asymmetry can be corrected by the scattered-wave deconvolution method of holographic imaging. The image created by the generalized

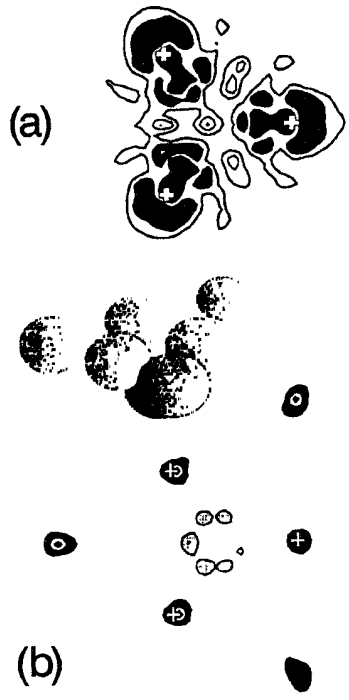


FIG. 3. Holographic image reconstructions of the atoms in the surface of a two-layer Cu(111) film, from a full multiple-scattering cluster calculation of the diffraction pattern. (a) The reconstruction using a simple phased Fourier integral, (b) the improvement using the deconvolution method described in the text. The model in the center shows some of the atoms in the cluster (the emitter and top layer atoms).

Fourier integral [Eq. (4)] can be seen in Fig. 3(b), applied to the same calculated diffraction pattern. The improvement in the image is dramatic. The local maxima are moved back to the correct locations of the atoms in the sample. The shaded regions of the contours in the deconvolved image are slightly larger than the diffraction limit (~0.5 Å diameter). In addition, the next-nearest-neighbor atoms, which are invisible in the ordinary transform, become readily apparent in the deconvolution. The deconvolved image of Fig. 3(b) is produced in a single step, without prior knowledge of the atom positions. This is still a direct transform method, and an image of all near-neighbor atoms in the correct positions is created at the same time. Applications of the scattered-wave integral transform theory show that it corrects for image aberrations introduced by the anisotropy of the scattered object waves, as well as those due to the angular distribution of the emitted reference wave. It reduces to Barton's phased Fourier transform[9] in the case of $s$-wave reference and object waves.

## II. SCATTERED-WAVE INTEGRAL TRANSFORMS

The factor $a(\hat{\mathbf{k}})$ appearing in Eq. (4) is an apodizing function, that attenuates the diffraction pattern amplitude as $\hat{k}_x,\hat{k}_y \rightarrow |\mathbf{k}|$, to avoid oscillations in the Fourier transform due to the finite range of momentum in the data. This factor arises naturally in the way that we ordinarily process the data. Diffraction patterns are originally acquired as a function of momentum direction relative to the sample normal $\hat{\mathbf{n}}$. The normalized, oscillatory part of the photoelectron diffraction pattern in polar and azimuthal coordinates $\chi(\Theta_{\hat{\mathbf{n}}},\Phi_{\hat{\mathbf{n}}})$ is then projected into a plane using a change of variables equivalent to an orthographic projection:

$$\chi(k_{\parallel},\Phi_{\hat{\mathbf{n}}})d\hat{k}_x d\hat{k}_y = \cos\Theta_{\hat{\mathbf{n}}}\chi(\Theta_{\hat{\mathbf{n}}},\Phi_{\hat{\mathbf{n}}})d\Omega_{\hat{\mathbf{k}}} , \tag{5}$$

with

$$k_{\parallel} = k\sin(\Theta_{\hat{\mathbf{n}}}) .$$

With an apodizing function of $a(\Theta_{\hat{\mathbf{n}}})=\cos\Theta_{\hat{\mathbf{n}}}$, the Fourier-transform integral becomes[2,4]

$$\Phi(\mathbf{r}) = \int\int \frac{1}{\mathcal{F}(\mathbf{k},\mathbf{r})}\chi(\hat{\mathbf{k}}_x,\hat{\mathbf{k}}_y)e^{i\mathbf{k}\cdot\mathbf{r}}d\hat{k}_x d\hat{k}_y . \tag{6}$$

The purpose of the deconvolution factor $\mathcal{F}(\mathbf{k},\mathbf{r})$ is to correct for distortions in the holographic image $\Phi(\mathbf{r})$ that are due to the angular dependence of the atomic-scattering factor, as well as angular factors in the diffraction intensity $\chi(\hat{\mathbf{k}})$ due to the atomic photoemission matrix element for cases other than $s$-wave emitters. The deconvolution factor $\mathcal{F}(\mathbf{k},\mathbf{r})$ is derived from the functional form of the scattered waves by replacement of the scattering atom position vector $\mathbf{r}_j$ by the general position vector $\mathbf{r}$. In the case of $s$-wave emission, which is used to approximately model high-energy Auger diffraction,[7] $\mathcal{F}(\mathbf{k},\mathbf{r})$ is formed from the generalization of the atomic scattering factor to a 6 degree-of-freedom function: $f(\mathbf{k},\mathbf{r})$. The corrected Fourier integral of Eq. (4) is actually a special case of a more general imaging integral transform, that we now proceed to develop.

To illustrate the construction of the scattered-wave integral transform, consider the final-state wave function for photoemission from an atom at the origin single-scattering from a near neighbor located at $\mathbf{r}_j$,

$$\psi_{\text{tot}}(\mathbf{k}) = \psi_0(\mathbf{k}) + \psi_s(\mathbf{k},\mathbf{r}_j) . \tag{7}$$

The first term represents the emission from the emitter atom in the absence of the scattering neighbor, and plays the role of the reference wave in the holographic interpretation of photoelectron diffraction. Similarly, the scattered waves $\psi_s$ are the object waves.

The photoelectron diffraction pattern is formed from the angular dependence of the photocurrent, which is proportional to $|\psi_{\text{tot}}(\mathbf{k})|^2$. The component of the diffraction pattern $|\psi_{\text{tot}}|^2$ containing the holographic fringes is called the anisotropy,

$$\chi(\mathbf{k}) = \frac{|\psi_{\text{tot}}|^2 - |\psi_0|^2}{|\psi_0|^2} . \tag{8}$$

Various approximate experimental techniques are used to approximately determine the angular dependence of the reference wave $|\psi_0|^2$.[4,12]

Given the definition of Eq. (8) the single-scattering anisotropy can be written

$$\chi_s(\mathbf{k}) = \frac{\psi_s}{\psi_0} + \frac{\psi_s^*}{\psi_0^*} + \frac{|\psi_s|^2}{|\psi_0|^2} . \tag{9}$$

The Fourier transform of the first term of this expression produces the "direct" holographic image of the scattering atom. The second term above leads to the "twin" image, and the third term has low angular-frequency components that contribute to artifacts in the image at small radii.[4]

In the simplest case, for which both the direct (reference) wave $\psi_0$ and the scattered (object) waves $\psi_s$ are $s$-like, the reconstruction integral of Eq. (1) produces "ideal" images of atoms at the correct locations (see below).[5,7] Deviations of both the reference wave and the object waves from $s$-like angular dependence lead to image aberrations in the reconstruction. Thus, we can use the functional form of the image term in Eq. (9) as a guide to create a "test function," which will be compared to the actual hologram (or diffraction pattern) of the sample.

This "test function" is found by replacing the specific atom-position vector $\mathbf{r}_j$ in the scattered wave $\psi_s(\mathbf{k},\mathbf{r}_j)$ of Eq. (9) by the general vector $\mathbf{r}$. We form a new function from the scattered waves and the reference waves

$$\Psi_{\text{ref}}(\mathbf{k},\mathbf{r}) = \frac{\psi_s(\mathbf{k},\mathbf{r})}{\psi_0(\mathbf{k})} . \tag{10}$$

It is important to stress that this is now a generalized function of both momentum and position with 6 degrees of freedom, and it does not depend on knowledge of a specific atom location.

We use the generalized scattered wave of Eq. (10) as a kernel for an image reconstruction integral. This is given by

$$r\Phi(\mathbf{r})=\int a(\hat{\mathbf{k}})[\Psi_{\mathrm{ref}}(\mathbf{k},\mathbf{r})]^{-1}\chi(\hat{\mathbf{k}})d\Omega_{\hat{\mathbf{k}}} . \quad (11)$$

This result forms the basis for a series of progressively more complex integral transforms for creating images from diffuse electron diffraction patterns. In the case of $s$-wave reference and object waves, it reduces to the phased Fourier transform derived by Barton.[9] For $s$-wave emitters, but including the angular dependence of the scattered waves, Eq. (11) reduces to the scattering-factor deconvolution Fourier integral [Eq. (4)] whose use has been described earlier.[3,7]

Under both the plane-wave approximation and the spherical-wave-corrected point-scatterer approximation, the scattered-wave integral transform will have the form of a generalized phased Fourier transform, shown in Eq. (4). Therefore, for convenience, we refer to these specializations of the integral transform of Eq. (11) as the scattered-wave-included Fourier transform SWIFT. The definition of the integral transform has been made in terms of an image function $r\Phi(\mathbf{r})$ in order to maintain consistency with previous usages of image functions.[1,6,9,23]

In the simple case of an $s$-wave emitter and scatterer, the scattered-wave kernel is easily seen to be

$$\Psi_{\mathrm{ref}}(\mathbf{k},\mathbf{r})=f_0\frac{e^{ikr}}{r}e^{-i\mathbf{k}\cdot\mathbf{r}} , \quad (12)$$

where $f_0$ is the $s$-wave atomic-scattering factor for the scattering atom. Substitution into Eq. (11) gives

$$\Phi(\mathbf{r})=e^{-ikr}\frac{1}{f_0}\int a(\hat{\mathbf{k}})\chi(\mathbf{k})e^{i\mathbf{k}\cdot\mathbf{r}}d\Omega_{\hat{\mathbf{k}}} , \quad (13)$$

which is identical to Barton's phased Fourier integral [Eq. (1)], except for the additional complex factor that depends on the magnitude of the momentum (or energy).

In the case of an $s$-wave emitter, but now allowing for anisotropic scattering from the object atom at position $\mathbf{r}_j$, the single-scattering wave function can be written in the form

$$\psi_{\mathrm{tot}}=\psi_0\left[1+f(\mathbf{k},\mathbf{r}_j)\frac{e^{ikr_j}}{r_j}e^{-i\mathbf{k}\cdot\mathbf{r}_j}\right] , \quad (14)$$

where the scattering factor $f(\mathbf{k},\mathbf{r}_j)$ can obtain spherical-wave corrections. By inspection, the second term of this approximate wave function generates the scattered-wave kernel function $\Psi_{\mathrm{ref}}$ by the replacement of $\mathbf{r}_j$ with the general vector $\mathbf{r}$. After substitution into Eq. (11) this simplifies, through the change of variables discussed above, to

$$r\Phi(\mathbf{r})=re^{-ikr}\int\int\frac{1}{f(\mathbf{k},\mathbf{r})}\chi(\hat{k}_x,\hat{k}_y)e^{i\mathbf{k}\cdot\mathbf{r}}d\hat{k}_x d\hat{k}_y . \quad (15)$$

This is the deconvolution integral that we have previously used to correct for the atom shift and asymmetry introduced by the atomic scattering factor, for diffraction patterns of an $s$-emitter (such as the high-energy Auger hologram of Fig. 2).[3] Notice that the scalar phase factor $e^{-ikr}$, which is important in filtering out multiple-scattering path contributions to holograms averaged over several energies, arises in a natural way in this treatment.[3,7,16,24]

An alternative way of describing the generalized Fourier integral [Eq. (4) above, or Eq. (15)] makes use of the "radial image function" concept.[2–4] The image function is viewed as a transform relative to a coordinate system that is not fixed with respect to the crystal, but rotates in image space. All angles are then referenced to the direction $\hat{\mathbf{r}}$ in image space. For example, rewriting Eq. (4) in the case of an $s$-wave emitter with a plane-wave scattering factor we have

$$\Phi(r,\hat{\mathbf{r}})=e^{-ikr}\int\frac{1}{f(\cos\theta_{\hat{\mathbf{r}}})}\chi(\theta_{\hat{\mathbf{r}}},\phi_{\hat{\mathbf{r}}})e^{ikr\cos\theta_{\hat{\mathbf{r}}}}d\Omega_{\hat{\mathbf{r}}} , \quad (16)$$

where the explicit dependence of angles on the direction in image space is shown. This way of writing the transform, in which $|\mathbf{r}|$ and $\cos\theta_{\hat{\mathbf{r}}}$ appear as transform pairs, makes the idea of a "deconvolution factor" more apparent.

## III. CONSTRUCTION OF SCATTERED-WAVE KERNELS

For $s$-wave emitters, the deconvolution factor that appears in the denominator of Eqs. (15) and (6) has been calculated using both the plane-wave atomic scattering factor,

$$f_{\mathrm{PW}}=\frac{1}{k}\sum_l(2l+1)e^{i\delta_l}\sin\delta_l P_l(\hat{\mathbf{k}}\cdot\mathbf{r}) , \quad (17)$$

which depends on the relative direction of $\mathbf{k}$ and $\mathbf{r}$, and from the spherical-wave-corrected scattering factor,

$$f_{\mathrm{SW}}^{(0)}(\mathbf{k},\mathbf{r})=\frac{1}{k}\sum_l(2l+1)e^{i\delta_l}\sin\delta_l P_l(\hat{\mathbf{k}}\cdot\hat{\mathbf{r}})\times\sqrt{1+l(l+1)/2(kr)^2}\,e^{il(l+1)/2kr} . \quad (18)$$

Note that in the case of the spherical-wave-corrected scattering factor, the function $f_{\mathrm{SW}}^{(0)}$ depends on the magnitude of $\mathbf{r}$, in addition to the relative direction of $\mathbf{k}$ and $\mathbf{r}$. The expression for $f_{\mathrm{SW}}^{(0)}$ in Eq. (18) is from the high-energy limit of Rehr and Alber's separable Green's-function propagator theory for electron scattering, for the case of an $s$-wave emitter.[25] Equation (15) with a plane-wave scattering-factor correction [Eq. (17)] was used to create the images of Figs. 2–4 . Both the plane-wave and spherical-wave factors were used in the results shown in Fig. 5.

The calculated atomic scattering factor $f(\theta)=|f(\theta)|e^{i\psi(\theta)}$ for Cu is shown in Fig. 6. This calculation used the potential of Moruzzi, Janak, and Williams,[26] to determine 20 phase shifts. These (real) phase shifts were subsequently temperature corrected using a Debye-Waller factor for 300 K with a Debye temperature of 320 K.[27] Spherical-wave corrections were included using the approximation valid in the high-energy limit, as shown in Eq. (18).[28] At 914 eV and with a nearest-neighbor distance of 2.55 Å, $kr\sim40$, and so this approximation is well justified.

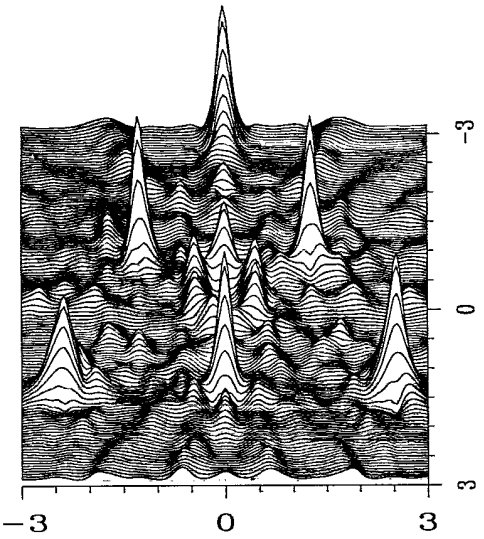


FIG. 4. Reconstructed image of a plane of Cu atoms from a cluster multiple-scattering calculation simulating a two-layer Cu(111) film. The diffraction pattern was the same as that used in Fig. 3. The reconstruction was done using the plane-wave scattered-wave deconvolution discussed in the text. Distances are in (Å).

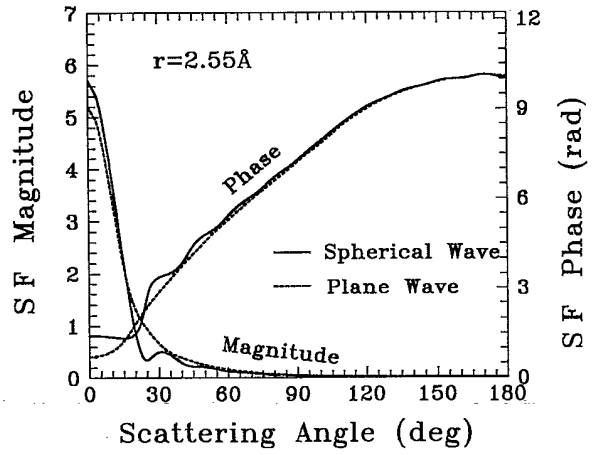


FIG. 6. Comparison of the plane-wave- and spherical-wave-corrected atomic scattering factor for Cu $LVV$ Auger electrons. The approximation used for the spherical-wave correction is discussed in the text. The angular dependence of the amplitude of the scattering factor, which has an approximate exponential shape, contributes to a broadening in the holographic image of an atom. The angular dependence of the phase leads to a shift in the atom position.

The scattered-wave deconvolution integral that results from the "test function" model, Eq. (15), differs from the definition given by Eq. (6) by a phase factor and the scalar prefactor $r$. The phase factor is necessary for combining holographic inversions at different energies.[24,16,3,7] In single-energy holograms, it is removed upon taking the modulus squared of the image function, $|\Phi(\mathbf{r})|^2$, whose intensity represents the holographic image. The prefactor of $r$ has a physical interpretation: it corrects for the $1/r$ decay of the outgoing electron reference wave. However, for the results shown here, we have used the definition of Eq. (6), so that the atomic image decreases in intensity away from the origin (see Fig. 5). As these techniques become better understood in terms of reliability, the use of $r^2|\Phi|^2$ may help improve the visibility of next-nearest-neighbor atoms, and suppress the remnant of the emitted reference wave at the origin.[8]

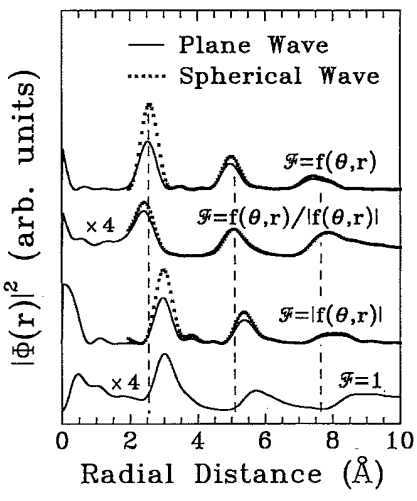


FIG. 5. Six different methods of image reconstruction are illustrated using the calculated diffraction pattern from a four-atom chain. The simple phased Fourier integral ($\mathcal{F}=1$) is at the bottom. The remaining curves show plane-wave and spherical-wave deconvolution factors using amplitude along, phase alone, or full scattering factor.

Relatively simple expressions for the scattered-wave kernel can be derived for higher angular momentum photoemission initial states in the plane-wave or point-scatterer approximations.[29,28] Following the formalism of Muster de Leon *et al.*,[29] the single-scattering final-state wave function can be written as an expansion in spherical harmonics,

$$\psi_{\mathrm{tot}}(\mathbf{k})=\sum_{L_f}\left[Y_{L_f}(\hat{\mathbf{k}})+e^{-i\mathbf{k}\cdot\mathbf{r}_j}\sum_{L}Y_L(\hat{\mathbf{k}})t_l G_{L,L_f}(\mathbf{r}_j)\right]A_{cL_f}\ , \tag{19}$$

where $A_{cL_f}\propto\langle\psi_{L_f}|\hat{\epsilon}\cdot\hat{\mathbf{r}}|\psi_c\rangle$ is the dipole matrix element between the core state and the final state of angular momentum $L_f$, $\hat{\epsilon}$ is the photon polarization vector, and $t_l=e^{i\delta_l}\sin\delta_l$ is the $t$ matrix for scattering from the neighbor atom. The double-scattering term that involves the $t$ matrix for the emitter, necessary for flux conservation in the single-scattering cross section,[28] has been left out since at high kinetic energy this backscattering term is very small.

In order to achieve atomic resolution in the reconstructed image, we require $kr_j\gg1$. This condition is the same as that used to justify the approximate form of the

Green's function,[28]

$$G_{L,L_f}(\mathbf{r})=4\pi\frac{e^{ikr}}{kr}Y_L^*(\hat{\mathbf{r}})Y_{L_f}(\hat{\mathbf{r}})c_l(kr)c_{l_f}(kr)\ . \tag{20}$$

The spherical-wave correction factors have the high-energy limiting form of

$$c_l=\sqrt{1+l(l+1)/2(kr)^2}e^{il(l+1)/2kr}\ . \tag{21}$$

Substitution of the Green's function (20) into Eq. (19) leads to the single-scattering spherical-wave-corrected wave function

$$\psi_{\rm tot}(\mathbf{k})=\sum_{L_f}A_{cL_f}\left[Y_{L_f}(\hat{\mathbf{k}})+\frac{e^{ikr_j}}{r_j}e^{-i\mathbf{k}\cdot\mathbf{r}_j}f_{\rm SW}^{(l_f)}(\mathbf{k},\mathbf{r}_j)\times Y_{L_f}(\mathbf{r}_j)\right], \tag{22}$$

where we use the spherical-wave-corrected atomic-scattering factor

$$f_{\rm SW}^{(l_f)}(\mathbf{k},\mathbf{r}_j)=\frac{1}{k}\sum_l(2l+1)t_lP_l(\hat{\mathbf{k}}\cdot\hat{\mathbf{r}}_j)c_lc_{l_f}\ . \tag{23}$$

From this expression, the scattered-wave kernel for primary photoemission from an $s$ state into a single $p$-wave final state is found using the same generalization procedure we have used earlier,

$$\Psi_{\rm ref}(\mathbf{k},\mathbf{r})=\frac{Y_1(\hat{\epsilon}\cdot\hat{r})}{Y_1(\hat{\epsilon}\cdot\hat{\mathbf{k}})}\frac{e^{ikr}}{r}e^{-i\mathbf{k}\cdot\mathbf{r}}f_{\rm SW}^{(1)}(\mathbf{k},\mathbf{r})\ . \tag{24}$$

In the scanned-angle geometry, this does not differ greatly from the expression found for $s$-wave emitters, since $\hat{\epsilon}\cdot\hat{\mathbf{k}}$ is a constant (the $\hat{\epsilon}\cdot\hat{\mathbf{r}}$ term is not constant, however). In terms of the generalized Fourier integral (4), the spherical-wave deconvolution function for an $s$ initial-state core level is simply

$$\mathcal{F}(\mathbf{k},\mathbf{r})=\frac{\hat{\epsilon}\cdot\hat{\mathbf{r}}}{\hat{\epsilon}\cdot\hat{\mathbf{k}}}f_{\rm SW}^{(1)}(\mathbf{k},\mathbf{r})\ . \tag{25}$$

Note that for both the PW (Ref. 30) and SW (Ref. 28) approximations, the scattered-wave kernel function factors into a structure factor times terms containing the scattering factor,

$$\Psi_{\rm ref}(\mathbf{k},\mathbf{r})=S(\mathbf{k}\cdot\mathbf{r})\mathcal{F}(\mathbf{k},\mathbf{r})\ , \tag{26}$$

where the structure factor is defined as $S=(1/r)\exp[ikr(1-\hat{\mathbf{k}}\cdot\hat{\mathbf{r}})]$. The two forms for the "deconvolution" factor $\mathcal{F}(\mathbf{k},\mathbf{r})$ are

$$\mathcal{F}(\mathbf{k},\mathbf{r})=\begin{cases}f_{\rm PW}(\mathbf{k}\cdot\mathbf{r})\dfrac{\sum_{L_f}A_{cL_f}Y_{L_f}(\hat{\mathbf{r}})}{\sum_{L_f}A_{cL_f}Y_{L_f}(\hat{\mathbf{k}})}, & \text{plane wave}\\ \dfrac{\sum_{L_f}A_{cL_f}f_{\rm SW}^{(l_f)}(\mathbf{k},\mathbf{r})Y_{L_f}(\hat{\mathbf{r}})}{\sum_{L_f}A_{cL_f}Y_{L_f}(\hat{\mathbf{k}})}, & \text{spherical wave}\ .\end{cases} \tag{27}$$

## IV. ANALYTICAL MODELS OF SCATTERED-WAVE IMAGE ABERRATIONS

It is worthwhile to consider some simple models of photoelectron holographic imaging that can be solved exactly. The stationary phase condition used by Barton[9] to justify the phased two-dimensional Fourier integral of Eq. (1) is exactly satisfied in the case of pure $s$-wave scattering. This corresponds to an angle-independent scattering factor $f=f_0e^{i\psi_0}$.

Consider the example of single scattering from an $s$-wave emitter at the origin by an atom at $\mathbf{r}=\mathbf{r}_j$, with the vector connecting the atom positions arranged to be parallel to the surface normal $\hat{\mathbf{n}}$, and the emitter atom below the scatterer. Assuming $f_0/r_j\le 1$, the diffraction pattern anisotropy is approximately $\chi(\hat{\mathbf{k}})=(2f_0/r_j)\cos[kr_j(1-\hat{\mathbf{k}}\cdot\hat{\mathbf{r}}_j)+\psi_0]$. For positions $\mathbf{r}$ parallel to the internuclear axis $\mathbf{r}_j$, the radial image function $\Phi(r\hat{\mathbf{r}}_j)$ can be evaluated using Eq. (1) (with $a=1$) to give

$$\Phi(\mathbf{r}=r\hat{\mathbf{r}}_j)=-2\pi\frac{f_0e^{i[k(r+r_j)/2+\psi_0]}}{r_j}\frac{\sin(kR/2)}{kR/2}+\text{twin}-\text{image term}\ , \tag{28}$$

where $R=r-r_j$ is the displacement vector of the image from the atom position, the twin-image term is given by the real term with $\mathbf{r}_j$ replaced by $-\mathbf{r}_j$. The modulus of the radial-image function for pure $s$-wave scattering has the "ideal image" form of

$$|\Phi(\mathbf{r})|^2=\left[\frac{2\pi f_0}{r_j}\right]^2\left[\left[\frac{\sin(kR/2)}{kR/2}\right]^2+\left[\frac{\sin(kR'/2)}{kR'/2}\right]^2\right], \tag{29}$$

where $R'=r+r_j$ is the location of the twin image, and cross terms from the square of Eq. (28) have been left out. The factor of $\frac{1}{2}$ in the argument of the sin $(kR/2)/kR$ function comes from integrating over only the half-sphere of electron emission outside the sample, which is accessible to experiment. The full width at half maximum (FWHM) of the ideal image function, along the radial direction, is approximately

$$\Delta r_{\rm FWHM}=\frac{4\sqrt{2}}{k}\ . \tag{30}$$

In the case of the 914-eV $LVV$ Auger line from Cu, this corresponds to an image full width of 0.37 Å.

To further illustrate the effects that the angular dependence of the atomic scattering factor has upon the holographic image, we construct an analytical model scattering factor of the form

$$\begin{aligned}&f(\theta)=|f(\theta)|e^{i\psi(\theta)}\ ,\\ &|f(\theta)|=f_0e^{-\alpha(1-\cos\theta)}\ ,\\ &\psi(\theta)=\beta(1-\cos\theta)+\delta\ .\end{aligned} \tag{31}$$

This form is chosen since it contains the essential ele-

ments of the shape of the scattering factor at high kinetic energy for copper, and it leads to a readily integrable image function. This simple functional form has two of the important characteristics of the atomic-scattering factor at high kinetic energy: the amplitude of the scattering factor is strongly peaked in the forward direction, and the phase depends strongly on scattering angle. By least-squares fitting to the actual spherical-wave, temperature-corrected scattering factor (Fig. 6), we find values of $\alpha \sim 25$, $\delta = 1.8$, $\beta = 5$, and $f_0 = 5.0$ a.u.

We can now substitute Eq. (31) into Eq. (9) and perform the Fourier integral [Eq. (1)] over the half-sphere representing photoemission outside the crystal. The result gives a radial image function whose leading terms are

$$|\Phi(\mathbf{r}=r\hat{\mathbf{r}}_j)|^2 = \left[\frac{2\pi f_0}{r_j}\right]^2 \left[\frac{1+e^{-2\alpha}-2e^{-\alpha}\cos[k(r-r_j)-\beta]}{\alpha^2+[k(r-r_j)-\beta]^2} + \text{twin-image term}\right] + \left[\frac{f_0}{r_j}\right]^2 \frac{1+e^{-4\alpha}-2e^{-2\alpha}\cos(kr)}{4\alpha^2+k^2r^2}\Bigg], \tag{32}$$

where again the twin-image term is found from the "image" term by the replacement of $r_j$ by $-r_j$. As $\alpha \to 0$ and $\beta \to 0$, this reduces to

$$|\Phi(\mathbf{r})|^2 = \left[\frac{2\pi f_0}{r_j}\right]^2 \left[\frac{\sin^2[k(r-r_j)/2]}{k^2(r-r_j)^2/4} + \text{twin-image term}\right] + (2\pi)^2 \left[\frac{f_0}{r_j}\right]^4 \frac{\sin^2(kr/2)}{k^2r^2/4}, \tag{33}$$

which is equivalent to the "ideal" image function for the case of pure $s$-wave scattering with an $s$-wave emitter, with the exception of the last term. In both cases we have again ignored small cross terms in evaluating $|\Phi(\mathbf{r})|^2$. The last term in (33) is smaller than the real image and twin image by the factor $(f_0/r_j)^2$, which was assumed to be small in the $s$-wave scattering case. This is not true for the forward-scattering geometry, and there is therefore a "forward-scattering artifact" that appears at or near $r=0$ (see also experimental examples in Ref. 4).

In the case of Cu at 914 eV, the factor $\alpha$ is quite large, so that the exponential terms in Eq. (32) can be neglected. In this limit the model image function [Eq. (32)] for an anisotropic atomic scattering factor has the approximate form of a Lorentzian function. The image function peaks at a radius of

$$r = r_j + \frac{\beta}{k}. \tag{34}$$

The full width of the image at half maximum is just

$$\Delta r_{\text{FWHM}} = 2\frac{\alpha}{k}. \tag{35}$$

This simple analysis has many of the important features of the full multiple-scattering simulations. First, note that the constant part of the phase $\psi(\theta)$, which was called $\delta$ and is equal to the forward-scattering phase shift, does not enter into the expression for either the atom position or the image shape. Instead, the cause of the atom shift is clearly due to the angular dependence of the scattering factor phase shift, with the dominant contribution coming from the $\cos\theta$ Fourier component which is proportional to the factor $\beta$. For Cu at 914 eV, the atom shift in this simple model is found to be $\delta r \sim \beta/k = 5/15.5$ Å $\sim 0.3$ Å. Considering the simplifications made in deriving these analytical results, this is in very good agreement with the results from full multiple-scattering simulations for atom chains[3] which show a shift of the order of $\sim 0.5$ Å. If the phase factor is fit only in the small-angle region below 45° scattering angle, the predicted atom shift is the same as that found in the multiple-scattering simulations. This means that an inspection of the atomic-scattering factor angular dependence may be used to determine the extent of the atom shift in a holographic reconstruction.

The broadening or peak width of the Lorentzian line shape is determined by the angular dependence of the amplitude of the scattering factor, as expressed by the parameter $\alpha$. Again using the appropriate values from the fit to the Cu scattering factor, we get an image width along the radial direction of $\Delta r = 2\alpha/k \sim 3$ Å. This is in general agreement with the elongated ellipsoidal tubes seen in forward-scattering images perpendicular to the sample surface.[1,2] The angular envelope of the amplitude part of the scattering factor also reduces the image intensity, by an amount $1/\alpha^2$, as compared to the ideal $s$-wave image.

In order to improve the resolution it is desirable to minimize the effects of the angular variation of both the amplitude (smaller $\alpha$) and phase (smaller $\beta$) of the scattering factor. This may be done by physically altering the experiment through different choices of electron energy, sample temperature, or scattering geometry, such as arranging to enhance backscattering instead of forward scattering. Alternatively, the effects of the scattering factor can be removed by the SWIFT generalized deconvolution procedures discussed here.

We have shown that a completely arbitrary phase shift produces no atom shift in the holographic image, so long as the angular dependence of the phase is small ($\beta \to 0$).

This is partly the reason that the holographic images of single-crystal samples have atoms in the correct positions, even though multiple-scattering effects are large in the forward-scattering geometry. As shown in Fig. 1, emitter atoms lying several layers below the surface do not contribute significantly to the forward-scattering peak along the internuclear axis. As more emitter atoms are added to the chain, the higher-order fringes at larger scattering angle are strengthened relative to the forward-scattering peak, since each atom has the same nearest-neighbor environment. These results confirm the results of previous calculations using a different formalism for embedded Cu chains.[31]

Since many different scattering paths can contribute to the final outgoing spherical wave from any particular subsurface atom in a single-crystal sample, the effective angular distribution of the phase tends to have less anisotropy than the single-scattering case. The reduction in the relative intensity of the forward-scattering peaks in single-crystal holograms also contributes to a reduction in the image full width, since the diffraction pattern intensity becomes effectively more isotropic. This can be seen in the experimental radial image functions from Cu(111),[2,3] which show an image full width of 0.4–0.5 Å, which is close to the diffraction limit. However, the intensity of the feature is weak.

## V. MULTIPLE-SCATTERING SIMULATIONS

The Lorentzian-like analytical model of a thin-film image reconstruction predicts several important features to be expected from a numerical simulation of the scattering.

(i) An arbitrary isotropic phase shift has no impact on the image, but the angular variation of the phase causes a shift in the apparent atom position. The direction of the shift is given by the sign of $\beta$, which measures the $(1-\cos\theta)$ dependence of the phase shift, and is positive for phase increasing with scattering angle.

(ii) The angular dependence of the amplitude of the scattering factor causes a broadening of the atomic image, or loss of resolution.

(iii) The angular dependence of the amplitude of the scattering factor reduces the intensity of the atomic image.

We expect these analytical results to be a guide in selecting suitable deconvolution factors for correcting aberrations in forward-scattering images. For example, (i) suggests that removing the phase dependence alone will shift the atom positions, but not affect the asymmetry or peak width. Similarly, from (ii) we expect that removal of the effects of the scattering factor amplitude on its own should correct the image asymmetry without moving the atom positions, and the image intensity should increase. Lastly, (ii) and (iii) imply that the image resolution and intensity can be improved by removal of the amplitude part of the scattering factor alone, but this will not shift the apparent position of the atomic images.

These concepts have been tested using a variety of image reconstruction integrals based on Eqs. (4) and (6). In order to include the strongest multiple-scattering effects that are present at high kinetic energy, calculations of the diffraction pattern from a linear chain of four copper atoms were used in these simulations. The atom spacing is 2.55 Å, to model the [110] nearest-neighbor direction in fcc copper. The multiple-scattering calculations were done using a cluster geometry and a formalism originally developed by Saldin and Pendry for low-energy electron diffraction,[20] and subsequently modified for photoemission, Auger electron, and Kikuchi electron diffraction calculations.[7] the diffraction patterns are calculated for $s$-wave emission from the atom at the end of the chain.

Seven different reconstruction algorithms are compared in the radial image-function plots shown in Fig. 5. The direction of image reconstruction is along the chain axis. The simple phased Fourier transform is represented by Eq. (4) with $\mathcal{T}=1$. This image function illustrates the basic aberrations that we have discussed. There is a shift in the local maximum for the nearest-neighbor atom of about 0.5 Å, and the shape of the peak is anisotropic, with a tail extending towards larger radii.

Six different deconvolution treatments are compared in the same figure. These are based on deconvolution of the scattering phase, the scattering amplitude, and the full scattering factor, for both a plane-wave and spherical-wave form of the scattering factor. The spherical-wave scattering factor used in the deconvolution is not the exact form, but rather the approximate form shown in Eq. (18). Since this expression is not valid at small radius, the deconvolution is truncated at 2 Å.

Removal of the effect of the amplitude of the scattering factor by deconvolution of $\mathcal{T}=|f(\theta,r)|$ is seen to increase the intensity of the atom images, and to largely remove the anisotropy of the atom image. However, the local maxima still are shifted from the expected position (shown by the dashed vertical lines). Notice that the spherical-wave deconvolution gives a larger image intensity than the plane wave. Since removal of the amplitude alone does not shift the atom positions, this technique may be useful when applied to single-crystal holographic images, or equivalently for thick films, which will already have atoms at the correct locations.

Deconvolution of the phase alone is accomplished with a factor $\mathcal{T}=f(\theta,r)/|f(\theta,r)|$. This causes a shift in the atom positions to smaller radius, while the anisotropy is largely still present. There is a smaller difference between the spherical-wave and plane-wave scattering fctor deconvolution in the phase correction. Notice that the near-neighbor atom position is overcorrected by the phase deconvolution. Furthermore, removal of the phase alone does not reduce the image width.

When the full scattering factor is used in the deconvolution integral, the image of the near-neighbor atom is shifted to the correct position, and the peak shape becomes fully symmetric. The intensity is also increased. Again, the spherical-wave factor provides an improvement in intensity as compared to the plane-wave deconvolution. Notice, however, that the atom positions of the next two atoms in the chain are overcorrected slightly by this process. This is due to the same multiple-scattering effects that result in single-crystal images having atoms at the right position. The scattered wave emanating from

atoms further down the chain are less forward-peaked than the near-neighbor scattered waves. In particular, the effective angular dependence of the phase of the second and third atoms from the emitter is more isotropic, so that when the phase correction is applied these atoms are shifted too far towards the origin.

The behavior of the deconvolution method as applied to strong forward scattering along atom chains confirms each of the features found in the analytical model: the atom shift, image asymmetry, and intensity loss.

## VI. APPLICATIONS

Perhaps the most important feature of the structure of the general transforms Eqs. (11) and (4) is that they preserve the direct inversion of diffraction patterns, and produce a complete three-dimensional image without the need for *a priori* judgments about atom positions (cf. the methods in Refs. 5 and 6, which require a knowledge of the location of bond directions).

In some cases, it may be possible to determine the bond directions of an unknown structure from inspection of the diffraction pattern. This is often true if a "reference" diffraction pattern can be obtained.[4] However, it is not always easy to identify the forward-scattering directions in a photoemission diffraction pattern, even for a relatively simple system such as an ultrathin film. As an example, in Fig. 7 we show the experimental diffraction pattern from an epitaxial fcc Cu(111) film grown on an Ir(111) single crystal. This film was determined to have between four and six layers of copper atoms, so that only three to five layers of emitter atoms are contributing to the diffraction pattern (the outermost layer contributes no significant features to the diffraction pattern).[3] In the fcc (111) stacking sequence, atoms in each layer have the same near-neighbor environment. Since the holographic inversion process is linear, a superposition of the diffraction patterns from each layer simply adds intensity at identical atom locations. The holographic image reconstructed from this data has been reported in Ref. 3.

The Auger diffraction pattern from Cu/Ir(111) film shows many symmetrical lobes of roughly the same intensity. Without addition information, it can be difficult to separate out the peaks that are due to forward scattering along internuclear axes from the higher-order interference peaks, a step required by the image-improvement techniques of Thevuthasan *et al.*[5] and Tong *et al.*[6]

Fortunately, the scattered-wave deconvolution method does not require such prior knowledge. As shown in the reconstructions of Fig. 3, a complete three-dimensional image is created as a direct output of the application of the Fourier integral in the form of Eq. (4) and Eq. (6).

The correction of both the absolute position of the image maximum and the line shape are together important to the accuracy of the holographic reconstruction. Since it is possible to obtain symmetrical peaks at the correct atom sites, the effective resolution will be smaller than the full width at half maximum of the $\sin^2(kR/2)/R^2$ function. The simulations shown in Figs. 5 and 3 suggest that the absolute accuracy of holographic images taken with near-kilovolt energy electrons may reach 0.1 Å. To illustrate this, we show the corrected image of the Cu(111) bilayer simulation in a different form in Fig. 4.

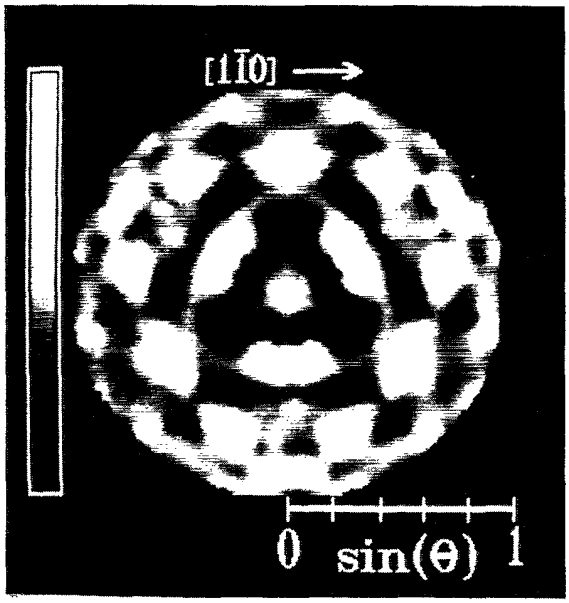


FIG. 7. X-ray excited Auger electron diffraction pattern from a 4–6-monolayer-thick fcc Cu(111) oriented epitaxial film on Ir(111). The diffraction pattern is shown in stereographic projection, so that pattern is shown as a function of $\hat{k}_x$ and $\hat{k}_y$. The boundary of the pattern corresponds to a maximum momentum of $|\mathbf{k}|=15$ Å$^{-1}$.

In addition to accuracy of atom image reconstructions, the *fidelity* of the image is important. That is, there should be peaks at the right-atom positions, but just as well there should not be "false-atom" peaks at the wrong places. This is an important distinction between the holographic transformation of angle-dependent diffraction patterns, and the one-dimensional Fourier transform of energy-dependent photoelectron diffraction data (sometimes called EDPD, for energy-dependent photoelectron diffraction).[32] The Fourier transform of EDPD data has peaks at every scalar path-length difference, which can result in a considerable number of peaks for even a simple system.[33]

In very great contrast, the holographic radial image function for *s*-wave scattering has peaks at only the correct atom locations, even in the presence of multiple scattering.[7] When forward scattering modifies the angular distribution, additional peaks are introduced at small radius in the radial image function.[4] Such features have been seen in the single-crystal data from Cu(100) and Cu(111).[1,2,4] They can also be seen at small radius in the atom-chain calculations of Fig. 5. Some of these small-radius features have been shown to arise from the forward-scattering peaks, which contribute to the Fourier integral as very large wave-vector psuedofringes [see the "artifact" terms in Eqs. (32) and (33)].

Satellite peaks lying between atom positions have been

seen, for example, in planar image reconstructions of Cu(100) holograms.[2] These appear to be primarily due to cross terms of the form $\psi_s(\mathbf{r}_j)\psi_s^*(\mathbf{r}_k)$ from the interference of scattered waves from two different atoms (the "intermodulation noise"[23]). When forward scattering is strong, these terms tend to be small because the overlap in angle or momentum space of scattered waves from different bond axes is small. In the case of $s$-wave scattered waves, these terms will be of order $(f_0/r_j)$ smaller in intensity than the atom image, so that satellite features, though present, should be smaller than the atom image in both limits.[34] This is an encouraging sign of the fidelity of the holographic reconstructions.

## ACKNOWLEDGMENT

This work was supported by the National Science Foundation, Grant No. DMR-88-05171.

[1]G. R. Harp, D. K. Saldin, and B. P. Tonner, Phys. Rev. Lett. **65**, 1012 (1990).

[2]G. R. Harp, D. K. Saldin, and B. P. Tonner, Phys. Rev. B **42**, 9199 (1990).

[3]S. Hardcastle, Z.-L. Han, G. R. Harp, B. L. Chen, D. K. Saldin, and B. P. Tonner, Surf. Sci. Lett. **245**, L190 (1991).

[4]Z.-L. Han, S. Hardcastle, G. R. Harp, H. Li, X.-D. Wang, J. Zhang and B. P. Tonner, Surf. Sci. (to be published).

[5]S. Thevuthasan, G. S. Herman, A. P. Kaduwela, R. S. Saiki, Y. J. Kim, and C. S. Fadley (unpublished).

[6]S. Y. Tong, C. M. Wei, T. C. Zhao, H. Huang, and H. Li, Phys. Rev. Lett. **66**, 60 (1981).

[7]D. K. Saldin, G. R. Harp, B. L. Chen, and B. P. Tonner (unpublished).

[8]The intensity precisely at the origin is identically zero, since we normalize the diffraction pattern to $\int \chi(\mathbf{k})d\hat{k}_x d\hat{k}_y = 0$. However, this leads to an apparent "peak" near the origin from the incompletely removed reference wave (see Fig. 5).

[9]John J. Barton, Phys. Rev. Lett. **61**, 1356 (1988).

[10]C. S. Fadley, in Proceedings of the 15th International Conference on X-ray and Inner Shell Processes, AIP Conf. Proc. No. 215 (AIP, New York, 1990).

[11]B. P. Tonner and Z.-L. Han (unpublished).

[12]H. Li and B. P. Tonner, Phys. Rev. B **37**, 3959 (1988); **40**, 10241 (1989).

[13]W. F. Egelhoff, Jr., Crit. Rev. Solid State Mater. Sci. **16**, 213 (1990).

[14]C. S. Fadley, in *Synchrotron Radiation Research: Advances in Surface Science,* edited by R. Z. Bachrach (Plenum, New York, 1990).

[15]S. A. Chambers in *Advances in Physics,* edited by S. Doniach (Taylor and Francis, London, 1991).

[16]B. P. Tonner, Ultramicroscopy (to be published).

[17]There are two conditions under which the extension of the Fourier integral (1) to include the angular space "inside" the crystal may be approximately allowed. At high kinetic energy, the forward-scattering effect limits the angular range of the diffraction pattern, so that for bond directions well removed from the surface, it is possible to set $\chi(\hat{\mathbf{k}})=0$ inside the crystal. In other special cases, the emitted atom and near neighbors may have a plane of symmetry or an inversion symmetry, so that the anisotropy inside the crystal can be derived from the measured diffraction pattern by $\chi(k_x,k_y,-k_z)=\chi(k_x,k_y,k_z)$ or from $\chi(k_x,k_y,-k_z)=\chi(-k_x,-k_y,k_z)$.

[18]B. E. Warren, *X-ray Diffraction* (Addison-Wesley, Reading, 1969), Chaps. 1 and 9.

[19]S. Kono, S. M. Goldberg, N. T. F. Hall, and C. S. Fadley, Phys. Rev. B **22**, 6085 (1980).

[20]D. K. Saldin and J. B. Pendry, Surf. Sci. **162**, 941 (1985).

[21]D. D. Vvedensky, D. K. Saldin, and J. B. Pendry, Comput. Phys. Commun. **40**, 421 (1986).

[22]The sign convention used for the Fourier transform in Eq. (1) and elsewhere in this paper is chosen to make the direct holographic image result from terms proportional to the atomic scattering factor, rather than its complex conjugate. The opposite convention (see, for example, Refs. 9 and 23) results from the interpretation of the transform as a resulting from an application of the Helmholtz-Kirchhoff integral.

[23]D. K. Saldin and P. L. de Andres, Phys. Rev. Lett. **64**, 1270 (1990).

[24]J. J. Barton, J. Electron. Spectrosc. Rel. Phenom. **51**, 37 (1990).

[25]J. J. Rehr and R. C. Albers, Phys. Rev. B **41**, 8139 (1990).

[26]V. L. Moruzzi, J. F. Janak, and A. R. Williams, *Calculated Electronic Properties of Metals* (Pergamon, New York, 1978).

[27]J. B. Pendry, *Low Energy Electron Diffraction* (Academic, London, 1974).

[28]M. Sagurton, E. L. Bullock, R. Saiki, A. Kaduwela, C. R. Brundle, C. S. Fadley, and J. J. Rehr, Phys. Rev. B **33**, 2207 (1986).

[29]J. Mustre de Leon, J. J. Rehr, C. R. Natoli, C. S. Fadley, and J. Osterwalder, Phys. Rev. B **39**, 5632 (1989).

[30]P. A. Lee, Phys. Rev. B **13**, 5261 (1976).

[31]M.-L. Xu, J. J. Barton, and M. A. Van Hove, Phys. Rev. B **39**, 8275 (1989).

[32]D. H. Rosenblatt *et al.*, Phys. Rev. B **26**, 1812 (1982).

[33]M. Sagurton, E. L. Bullock, and C. S. Fadley, Phys. Rev. B **30**, 7332 (1984).

[34]Some examples of satellite structure in simulated reconstructions of $s$-wave scattering holograms are shown in Ref. 5, as a function of the magnitude of the ratio $f_0/r_j$ is varied.